FULL ARTICLE

Photoluminescence intensity ratio of Eu-conjugated lactates—A simple optical imaging technique for biomarker analysis for critical diseases

Tarun Kakkar[1] | Nikita Thomas[2] | Eric Kumi-Barimah[1]* (iD) | Gin Jose[1] | Sikha Saha[2]

[1]School of Chemical and Process Engineering, University of Leeds, Leeds, UK

[2]Leeds Cardiovascular and Metabolic Medicine, Faculty of Medicine and Health, University of Leeds, Leeds, UK

*Correspondence
Eric Kumi-Barimah, School of Chemical and Process Engineering, University of Leeds, Clarendon Road, Leeds LS2 9JT, UK.
Email: e.kumi-barimah@leeds.ac.uk

Funding information
Engineering and Physical Sciences Research Council, Grant/Award number: EP/M015165/1; EPSRC, Grant/Award number: EP/M015165/1; EPSRC-IAA

Instant measurement of elevated biomarkers such as lactic acid offers the most promising approaches for early treatment and prevention of many critical diseases including cardiac arrest, stroke, septic shock, trauma, liver dysfunction, as well as for monitoring lactic acid level during intense exercise. In the present study, a unique dependence of visible photoluminescence of Eu^{3+} ions resulting from $^5D_0$ to $^7F_{J(J = 0,1,2,3,4)}$ transitions, which can be exploited for rapid detection of biomarkers, both in vitro and ex vivo, has been reported. It is observed that the integrated intensity ratio of photoluminescence signals dominating at 591 and 616 nm originating from $^5D_0$ to $^7F_2$ and $^5D_0$ to $^7F_1$ transitions in Eu^{3+} ions can be used as a biosensing and bioimaging tool for detection of biomarkers released at disease states. The Eu^{3+} integrated photoluminescence intensity ratio approach reported herein for optical detection of lactates in blood serum, plasma and confocal imaging of brain tissues has very high potential for exploitation of this technique in both in vitro monitoring and in vivo bioimaging applications for the detection of biomarkers in various diseases states.

KEYWORDS
bioimaging, biomarkers, brain tissue, europium nitrate, fluorescence, integrated photoluminescence ratio, L-lactic acid, plasma, serum
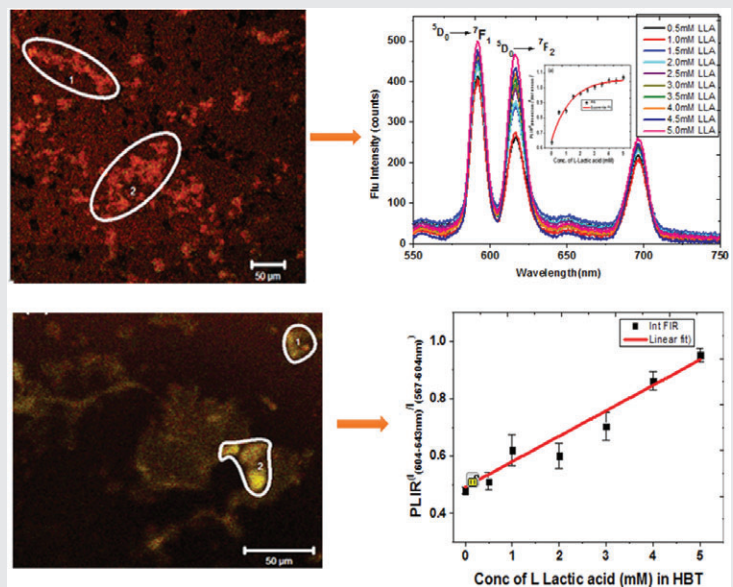
1 | INTRODUCTION

Chronic diseases such as cancer, ischemic heart disease, diabetes, stroke and lung disorders are among the top 10 causes of morbidity in the world [1]. With the onset of these diseases, various biomarkers are produced in the body such as free fatty acid, phospholipases and lactates [2, 3]. So as to fathom the severity of disease, hence to provide earlier treatments, it is essential to determine the elevated levels of biomarkers [4]. Lactate plays a significant role in various metabolic cycles in the body including Cori cycle and Krebs cycle [5–7]. The normal lactate concentration in human blood plasma is 0.3 to 1 mM and increased lactate levels indicate possible error in cellular metabolism [3]. Accumulation of lactic acid in the muscle occurs during exercise of relatively high intensity, and is often related to fatigue. Lactate levels in clinical practice are used to measure illness severity and also to gauge response to therapeutic interventions. Increased concentration of lactate is observed in the human brain during ischemic stress conditions. This is based on the fact that energy production shifts from aerobic to anaerobic pathway leading to slow clearance of lactates [8]. Ischemic cardiac disease occurs due to myocellular hypoxia, a condition caused by insufficient supply of oxygen to the myocytes in heart muscles, resulting from acute injury due to embolism or plaque formation [9]. This hypoxic injury causes disruption in functioning of mitochondria, shifting energy production in the cells from aerobic respiration to anaerobic pathways, leading to accumulation of lactates [10]. Hence, it is critical to estimate the release of lactates and other toxic metabolites due to ischemia in order to understand the cellular damage caused during several diseases including cardiovascular diseases, stroke and cancer [11]. Lactic acid levels are also elevated when the liver is severely damaged or diseased, because the liver breaks down lactic acid. Very high levels of lactic acid may cause a serious, sometimes life-threatening condition called lactic acidosis. Due to its key role in the human body, the development of a fast response and user-friendly methods of lactic acid measurement is essential.

Currently, there are very few methods for early diagnosis of these critical disorders, highlighting the need for a method for rapid identification of potential biomarkers released during these diseases, so that appropriate treatment can be provided at early stages. Recent advances in imaging techniques together with enzyme-linked immunosorbent assay (ELISA), proteomics and metabolic profiling have enhanced the feasibility of patient screening for the diagnosis with biomarkers [12]. However, it is not suitable for "point-of-care" at home for the patient or at the general practice, allowing early diagnosis that should benefit in preventing irreversible physiological damage, thus precluding from pathogenesis. Also, these current techniques necessitate frequent collection of high volume of blood for tests, which are difficult to implement clinically in high-risk patients and in children. Currently, positron emission tomography modality combined with radioactive glucose tracer fluorodeoxyglucose (^{18}F) is used in medical imaging to detect the amount of lactate in the cancer affected region [13]. However, there are various implications related to this technique due to its restricted access to investigation area, expensive procedures, use of radioactive tracers and non-suitability to be applied in hyperglycemic patients [14]. Besides this, photoacoustic imaging modality has also been investigated extensively by using various photoacoustic contrast agents comprising dye and nanoparticles to visualize the structure and function of biological tissues for biomedical and biomedicinal applications [15–17]. For instance, Zhong et al. [16] studied photoacoustic treatment and imaging of human epithelial carcinoma (HeLa) tumor cells in vivo by utilizing contrast therapeutic agents such as single-walled carbon nanotubes, indocyanine green containing nanoparticles (ICG-PL-PEG) and gold nanorods (AuNRs) conjugated with folic acid.

Trivalent rare earth (RE) elements are characterized by their $(4f^n)6s^2$ electronic configuration and have been actively investigated for biomedical applications [18–20]. The above electronic configuration allows their functionalization with weak acids and polar organic systems near neutral to acidic pH. The complexation of lactate with RE elements such as neodymium (III) (Nd^{3+}) and europium (III) (Eu^{3+}) was reported by Guoxin et al. [21]. Eu^{3+} complexes have been identified as novel materials for quantifying anion concentrations such as lactate, citrate, bicarbonate and urate using emission bands in the red wavelength (>613 nm) and their fluorescence intensity ratios [22–24]. The most stable and common valence state of RE ions is 3+, although some do have 4+ and 2+ states also. The electronic shielding of $4f^n$ level electrons with $6s^2$ weakens RE ions' interaction with their organic/inorganic host and hence allows distinctive display of photoluminescence (PL), which not only reflects the optical properties of the ions but also their molecular environment, especially when PL is supplemented by the lifetime decay analysis while considering its biosensing and bioimaging applications. The europium ions ($Eu^{2+/3+}$) are specific for their sensitivity to chemical environment which affects the oscillator strength of optical transitions, and consequently emit different proportions of light when excited using a coherent light source (eg, a laser). Therefore, Eu^{3+} ions are proposed as a credible alternative to organic molecules since organic molecules undergo autodegradation which is not suitable when biosensing or bioimaging application is considered [25, 26]. On the other hand, upconversion PL of lanthanide-doped nanoparticles has attracted great research attention and is used in many studies as well. This is another effective optical imaging method of biological cells and tissues due to its advantages, which include the absence of photodamage to living

organism, high light penetration depth in biological tissues and high detection sensitivity [27, 28].

A few studies focused on the toxicological effects of RE ions using human osteosarcoma cell line MG63, umbilical cord perivascular cell and mouse macrophages; reported large concentration or systemic accumulation of these ions could lead to acute pathology and cellular toxicity [29, 30]. However, these studies produce variable results. Therefore, it is important to test these ions in the biological system especially on human primary cells before they have been used in biosensing or bioimaging purposes.

In this paper, we report a novel methodology for analyzing Eu^{3+} ions conjugated with lactic acid in aqueous medium and rodent's brain tissue based on a photoluminescence intensity ratio (PLIR) approach using fluorescence measurements in the yellow and red wavelengths. This method can be employed to other biomarkers as well. Lactate exists in 2 isomers: L-lactate, produced as a result of anaerobic metabolism in human and D-lactate, byproduct of bacterial metabolism. Our lactate measurements only include L-lactate, the primary isomer produced in humans. Our investigation focuses on the following aspects: (1) evaluation of the cytotoxicity of europium nitrates [Eu $(NO_3)_3$] on human primary cells, (2) determination of pH-dependent absorption spectra and PL excitation spectra of Eu-conjugated lactic acid, (3) analysis of the relative intensities of PL emissions of the Eu^{3+} ions results from $^5D_0$ to $^7F_1$ and $^5D_0$ to $^7F_2$ energy-level transitions occurring in the yellowish red region of the electromagnetic spectrum and (4) determination of the PLIR of the above 2 transitions as an approach for imaging lactates in biological samples and rodent tissues.

2 | MATERIALS AND METHODS

2.1 | Materials

Phosphate buffer saline (PBS), Dulbecco's modified Eagle's Medium/Ham's Nutrient mixture F12 (DMEM), antibiotics (Penicillin-Streptomycin), L-glutamine, NaOH pellets (99.99%), HCl (36%-38%), lactic acid solution (85%), Tris(tris(hydroxymethyl)aminomethane) buffer (99.9%) and poly-D-lysine hydrobromide were purchased from Sigma-Aldrich (Dorset, UK), while fetal bovine serum (FBS) of South American Origin was obtained from Labtech.com. Phospholipid (L-α-lecithin from egg yolk, 98%) was obtained from Calbiochem, Merclifesciences, (Merck, Kenilworth, New Jersey). New born calf serum was obtained from Biosera, Essex, UK. Europium nitrate hexahydrate ((Eu(NO_3)_3.6H_2O), 99.9%) was obtained from Alfa Aesar, (Heysham, Lancashire UK). Europium nitrate dissolved in water was used as a precursor solution for Eu^{3+} conjugation with lactic acid, cells and rodent tissues.

2.2 | In vitro cell culture and cell viability test

Human primary brain astrocytes were purchased from ScienCell (Carlsbad, CA, USA). Astrocytes were cultured in F12 (DMEM) medium, supplemented with 10% sterile-filtered FBS of South American Origin, 1% antibiotics (Penicillin-Streptomycin) and 1% L-glutamine at 37°C in 95% air and 5% CO_2. Cells were supplemented with fresh media every 3 to 4 days, depending on the requirements, until confluency was achieved. The cells were then transferred to 24-well plates filled with poly-L-lysine, rinsed with PBS and treated with Eu(NO_3)_3. Cell viability was assessed using the 3-(4,5-dimethylthiazol-2-yl)-2,5-diphenyltetrazolium bromide (MTT, Sigma, Thermo Fisher Scientific (Life Technologies) PaisleyPA4 9RF, UK) reduction assay as described previously [28–30]. Absorbance of the cells was measured using a spectrophotometer at a test wavelength of 570 nm and a reference wavelength of 630 nm. Student's t test (unpaired) was used to determine the significance of differences between means, with P values <.05 being considered significant. Cell viability was expressed as a mean percentage of absorbance of control cells $\pm$ SEM.

2.3 | Rodent tissue preparation

All experiments were performed on 12-week-old (25-30 g) male C57BL/6J mice (Harlan-Olac, Bicester, UK) weighing 24 to 26 g under appropriate UK Home Office personal and project licenses and adhered to regulations as specified in the Animals Scientific Procedures Act (1986). After a habituation period of 1 week, the mice were sacrificed by decapitation under halothane anesthesia. Small samples of brain tissue were carefully dissected, weighed and homogenized using tris-buffered saline. Different dilutions of Eu(NO_3)_3 in distilled water (1, 10, 100 μM) were added directly to homogenized brain tissue (HBT). Brain tissue treated with Eu^{3+} ions was kept on a shaker table for 24 hours at 40°C. The tissue samples were then mounted on slides, cover slipped using mounting medium and observed under laser confocal microscope (Zeiss LSM 510, Carl Zeiss, Heidelberg, Germany).

2.4 | UV-Vis absorption, fluorescence and PL spectroscopic experiment

The absorption spectra of europium ions (Eu^{3+}) in lactic acid and europium nitrate solution with varying pH were measured using Perkin-Elmer Lambda 19 DM UV/Vis/NIR spectrometer (PerkinElmer, Llantrisant UK). The initial solutions with low pH were prepared by adding 100 mM Eu(NO_3)_3 and 5 mM lactic acid. To increase the pH from 5 to 6, we added a small quantity of NaOH solution to it. The fluorescence excitation spectrum of 1 M Eu^{3+} ion in water at room temperature was recorded using FS920 Spectrofluorometer (Edinburgh Instruments, Livingston, UK) with visible photomultiplier tube detector. This experiment was performed to determine the fluorescent emission as well as excitation spectrum; xenon flash lamp with monochromator was used as excitation light source. In addition, 10 mM stock solutions of Eu(NO_3)_3.6H_2O and L-lactic acid were

prepared in distilled water (aqueous solution). Then, 1 mL working solution of 1 mM $Eu(NO_3)_3.6H_2O$ with different concentrations of L-lactic acid ranging from 0.5 to 5.0 mM in aqueous solution, serum and plasma were finally prepared for fluorescence studies. The sample solution in 10 mm pathlength cuvette was placed in a CUV-ALL-UV 4-way cuvette holder and excited with laser diode operating at 395 nm (module of KVANT Scientific) and a current of ~40 mA. A high-pass filter with a cut-on wavelength of 515 nm was employed between the cuvette and optical fiber charge-coupled device (CCD) array to block second-order wavelength and the short wavelength radiation. Fluorescence emission was focused onto the optical fiber CCD camera to the USB2000 spectrometer (Largo, FL, USA). Fluorescence spectra were recorded using Ocean Optics software (Largo, FL, USA) in the wavelength range of 550 to 850 nm to determine the calibration curve for L-lactic acid.
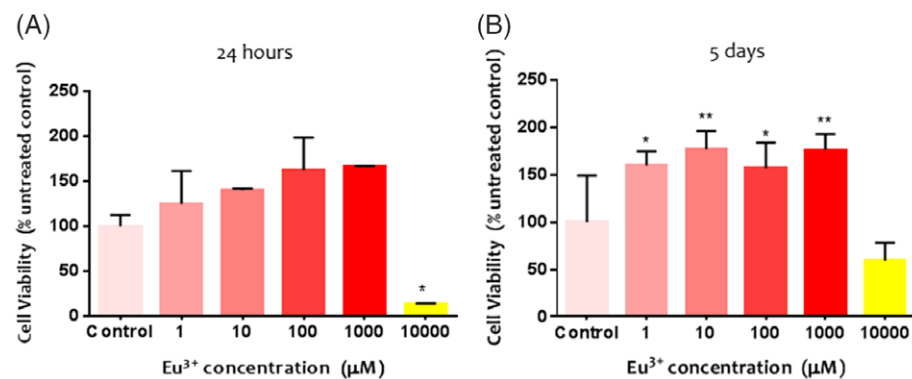
2.5 | Confocal laser scanning microscopy

Conjugation of europium with biological metabolites, lactate and phospholipids has been studied using a confocal laser scanning microscope Zeiss LSM 510 equipped with a diode laser at 405 nm, which excites the Eu^{3+} ions in the conjugated medium and produces a corresponding characteristic fluorescence spectrum in the visible wavelength region (570-650 nm).
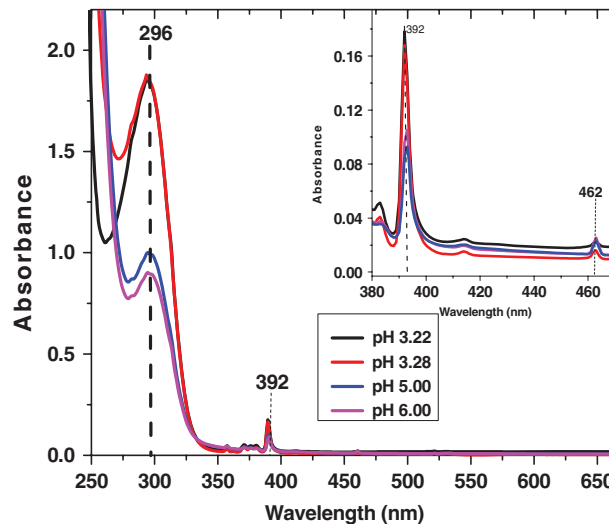
3 | RESULTS AND DISCUSSION

3.1 | Cell viability studies

Cytotoxicity of ions was determined in human astrocytes incubated in various concentrations of $Eu(NO_3)_3$ at 24 hours and 5 days, and is shown in Figure 1. This was performed to ensure that $Eu(NO_3)_3$ does not exert any toxicity on the biological tissue/fluid and can be used in biosensing. Student's t test (unpaired) was utilized to evaluate the significance of differences between mean values. The concentrations of $Eu(NO_3)_3$ from the control to 1000 μM in human astrocytes increase with the cell viability (expressed as %), followed by a rapid loss of cell viability at higher concentration (10 000 μM). After 5 days, the concentrations of $Eu(NO_3)_3$

FIGURE 2 pH-dependent absorption spectra of europium nitrate with lactic acid; inset shows those peaks with very low absorbance magnified

showed slightly increased cell viability which ranged from 10% to 40% (Figure 1B) as compared to Figure 1A. Thus, cytotoxicity studies signify that the Eu^{3+} ions are nontoxic at concentrations ranging from 1 to 1000 μM and to some extent are cytoprotective as cell viability is increased at these concentrations compared to the control. However, cell viability is deceased compared to the control when the concentration of Eu^{3+} ions is increased to 10 000 μM.

3.2 | Absorption spectroscopy of Eu^{3+} ion in solutions

The room temperature absorption spectra of 100 mM $Eu(NO_3)_3$ in lactic acid solution with varying pH are shown in Figure 2. This experiment was carried out to evaluate the binding mode of lactates with Eu^{3+} ion complexes. As we increase the lactic acid to $Eu(NO_3)_3$ solution ratio (pH 3.22 and 3.28), there is no notable change to the peak positions in absorption spectra while changing pH from 5 to 6; by adding NaOH solution, a hypochromic shift is observed, which is described in terms of decrease in absorption with rise in pH in all absorption peaks. It is important to point out that this decrease in the absorption is due to the formation of europium hydroxide upon addition of NaOH; therefore, the increased basicity around Eu^{3+} ions is responsible for such
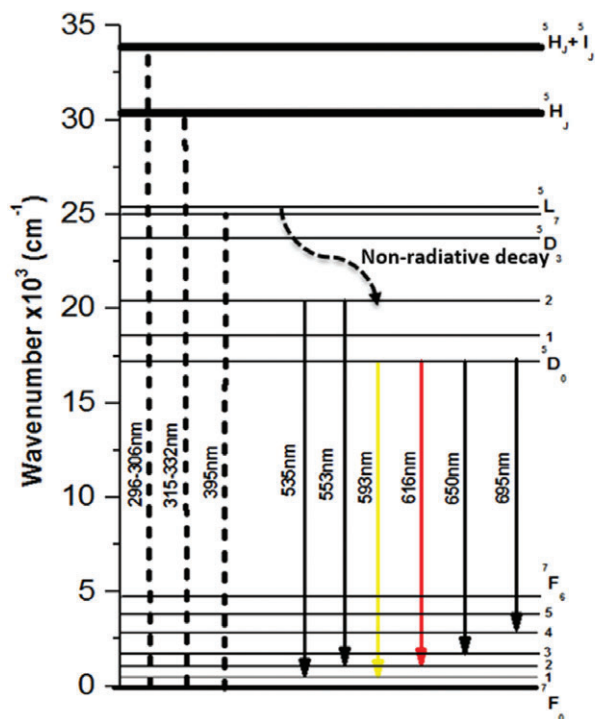

FIGURE 1 Comparative investigation of cell viability tests of human primary astrocytes incubated with europium nitrate for: A, 24 hours and B, 5 days. Significance levels: *P < .1; **P < .01

FIGURE 3 Energy level diagram of Eu^{3+} ions showing different absorption and emission transitions

FIGURE 4 Fluorescence excitation spectrum for 1 M europium nitrate for an emission wavelength of 616 nm

changes. The predominant peaks in the absorption spectrum are at 296 and 392 nm and they correspond to the transition from $^7F_0 \rightarrow {}^5D_4$ and $^7F_0 \rightarrow {}^5L_6$ levels as shown in Figure 3. The broad absorption band centered at 296 nm could be due to additional contribution from the weak $\pi^* \leftarrow n$ transition of the carboxylic group of lactic acid [31, 32]. An important aspect of the absorption spectroscopy of aqueous solutions is that the above 2 absorption peaks at 296 and 392 nm are always present in the range of pH studied in the current study. Henceforth, laser diode operating at 395 nm which is in close proximity to the absorption band of Eu^{3+} centered at 392 nm was utilized as excitation source for fluorescence measurements.

3.3 | Luminescence spectroscopy and optical sensing of biomarkers using PLIR

The excitation spectrum of the 1 mM aqueous $Eu(NO_3)_3$ was obtained as a reference for selecting the suitable excitation wavelengths for Eu^{3+}-conjugated lactate as a biomarker. The excitation spectrum of Eu^{3+} in aqueous solution recorded for a fixed emission wavelength of 616 nm is shown in Figure 4. The most prominent peak is at 395 nm and this wavelength has been used as wavelength of excitation for the measurement of luminescence spectrum. At 395 nm excitation, the Eu^{3+} ions in the medium are excited from the ground level $^7F_0$ to the energy level $^5L_6$ (as in the energy level diagram—Figure 3). As can be seen from the spectrum, there are other wavelengths of excitations which may also be used for Eu^{3+} containing medium. However, the $^7F_0$ to $^5L_6$ absorption is known to be less dependent on the variations in the surrounding medium,

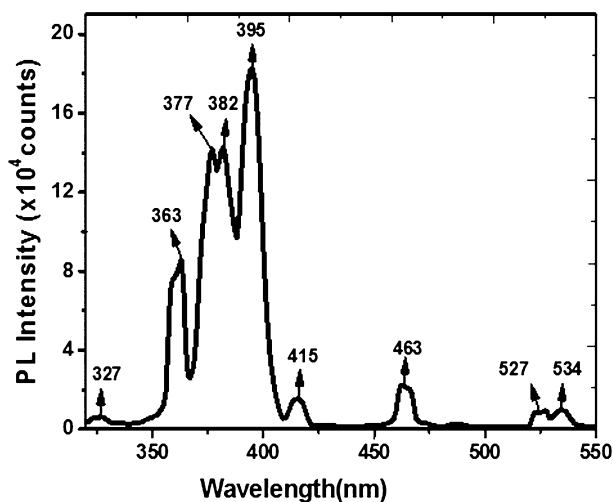hence optimized as the excitation wavelength for the current experiment [32]. Figure 5 shows that the emission peaks of Eu^{3+} ion conjugated with lactic acid that occurred at 591 nm ($^5D_0$ $^7F_1$) and 616 nm ($^5D_0$ $^7F_2$) are more intense, which represent the change in concentration of lactic acid in the micromolar range. Other PL emission bands present in Figure 5 are at 535 nm ($^5D_1$ $^7F_1$), 556 nm ($^5D_1$ $^7F_2$) and 650 nm ($^5D_0$ $^7F_3$); $^5D_0$ $^7F_4$ is possible at 696 nm.

PLIR measurement is a special technique that uses luminescence or fluorescence intensities from 2 closely spaced energy levels to monitor change in luminescence intensity ratio. The magnitude of luminescence intensity is dependent on both intrinsic properties of the compound and well controlled experimental parameters, comprising of the intensity of excitation source and concentration of the anion component of the compound. The change in the luminescence intensity I_F, as a function of concentration at low absorbance is given as [33, 34]:

$$I_F = \Phi I_o \left(1 - e^{-2.3\varepsilon_\lambda lc} \right), \tag{1}$$

where Φ is the fluorescence quantum efficiency, I_0 is the incident radiant power, ε_λ is the molar extinction coefficient which is wavelength dependent, l is the path length of the cell or cuvettes containing the sample and c is the molar concentration. Using MacLaurin series, the terms in the parenthesis of Eq. (1) can be expanded as follows [33]:

$$I_F = \Phi I_o \left(2.3\varepsilon_\lambda lc - \frac{(2.3\varepsilon_\lambda lc)^2}{2!} + \frac{(2.3\varepsilon_\lambda lc)^3}{3!} + \ldots \right) \tag{2}$$

It is important to point out that theoretically luminescence or fluorescence intensity vs concentration is not actually linear as shown in Eqs. (1) and (2). However, if the absorbance $2.3\varepsilon lc < {\sim}0.05$, then the higher order terms becomes insignificant [34]. Henceforth, at low concentrations the fluorescence intensity of a sample is approximately
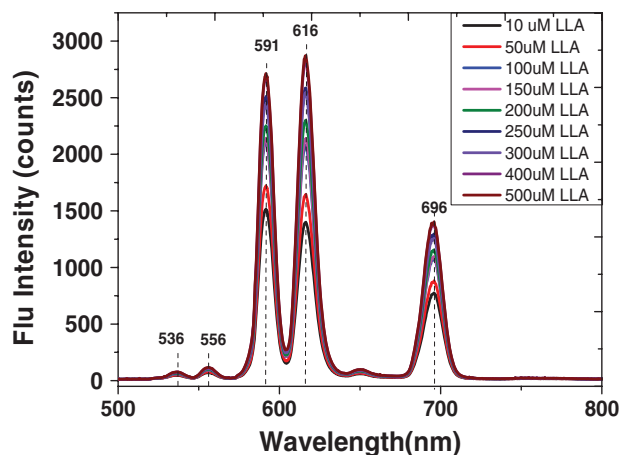
FIGURE 5 Fluorescence emission spectra of europium nitrate with lactic acid in lower concentration when excited at 395 nm
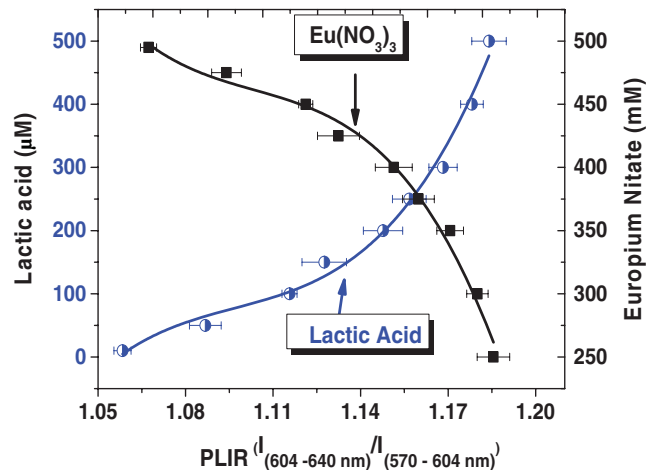

FIGURE 6 Photoluminescence intensity ratio corresponding to PLIR > 1 mol of lactic acid in solution (left *Y*-axis) and for mole fraction of europium nitrate in solution (right *Y*-axis)

linearly proportional to the concentration which is given by [34]:

$$I_F = 2.3\Phi I_o \varepsilon_\lambda l c \qquad (3)$$

In order to obtain a linear fluorescence response as a function of concentration, it is essential to maintain a concentration that has an absorbance ~0.1 or lower. It is worth mentioning that as the sample concentration increases, it reaches a point where fluorescence intensity eventually decreases, this is due to increases in the absorbance of the excited sample.

The 2 luminescence emissions bands, with peaks centered at 591 and 616 nm occur (Figure 5) when Eu^{3+} ions radiatively relax from $^5D_0$ level to $^7F_1$ and $^7F_2$ levels, respectively. The $^5D_0$ to $^7F_1$ (591 nm) transition is magnetic dipole (MD) allowed and is relatively unaffected by the chemical surroundings of the local site symmetry of Eu^{3+} ions, henceforth, very weak emission intensity. However, the $^5D_0$ to $^7F_2$ (616 nm) transition is allowed by the electric dipole (ED) transition. Consequently, the intensity of this ED transition is strongly dependent on the degree of mixed parity and, hence, there is lack of inversion symmetry at the Eu^{3+} site. Such differences in luminescence intensity of these 2 closely spaced transition bands allow easy analyses of PLIR [22, 24]. The PLIR defined by $I_{(604-640\ nm)}/I_{(570-604\ nm)}$ is the ratio of integrated intensity of ED transition to MD transition, and provides information about the distortion from local sites inversion symmetry of the Eu^{3+} ions in the ligand complex. The PLIR plotted in Figure 6 is always greater than unity at lower concentrations of lactic acid in the micromolar range, which is still detectable at ease. When fluorescence image is recorded under these conditions, such a medium will be predominantly reddish as shown in section 3.3.

Figure 7A-C illustrates the selected luminescence spectra of various concentrations of lactic acid ranging from 0.5 to 5.0 mM in 1 mM $Eu(NO_3)_3.6H_2O$ in aqueous solution and in biological fluids such as blood serum and blood plasma. From Figure 7A, it is clear that the spectra peaks

are predominant at 593 nm ($^5D_0 \rightarrow {}^7F_1$) electronic transition rather than 616 nm ($^5D_0 \rightarrow {}^7F_2$) transition. This indicates that Eu^{3+} ion is located at high symmetry sites [35], whereas Figure 7B shows luminescence spectra of the same concentrations of lactic acid in serum and 1 mM $Eu(NO_3)_3.6H_2O$ aqueous solution. This figure shows small change in luminescence intensities at 591 and 616 nm as compared to Figures 5 and 7A. Figure 7C shows lactic acid concentrations in 1 mM $Eu(NO_3)_3.6H_2O$ in the plasma. The emission signature centered at 616 nm transition is more predominant as compared to Figure 7A,B. It can be seen that as the lactic acid concentrations in the biological fluids increase, the fluorescence intensity also increases (Figure 7A) and decreases (Figure 8B,C) slightly. This noticeable quenching in Figure 7B,C in the luminescence intensity may be ascribed to the binding mode polarity, sensitive of Eu^{3+} linked to biological fluids and lactic acid, as well as OH vibration. Many studies have shown that Eu^{3+} luminescence peak at $^5D_0 \rightarrow {}^7F_1$ transition is relatively strong, and exhibited no/little change on the surrounding ligand environment due to its MD contribution [35–40]. Similarly, the $^5D_0 \rightarrow {}^7F_2$ electronic transition is predominantly electric dipole and the intensity is highly sensitive to the Eu^{3+} coordinate environment [31, 33–35] as mentioned above.

Using the luminescence emission spectra shown in Figure 7, calibration curves for Eu^{3+} ion conjugated with different concentrations of lactic acid in different biological fluids mentioned above were developed. The integrated PLIR of the 2 emission bands centered at 591 and 616 nm was implemented and recorded. These were plotted as a function of the concentrations of lactic acid and fitted with exponential function (integrated $0.60 \leq$ PLIR ≤ 1.06), linear function (integrated $0.089 \leq$ PLIR ≤ 0.95) and second-order polynomial function (integrated $2.50 \leq$ PLIR ≤ 2.75) depicted in Figure 8A-C. Figure 8D depicts the calibration graph constructed for L-lactic acid (mM) in 200 μM
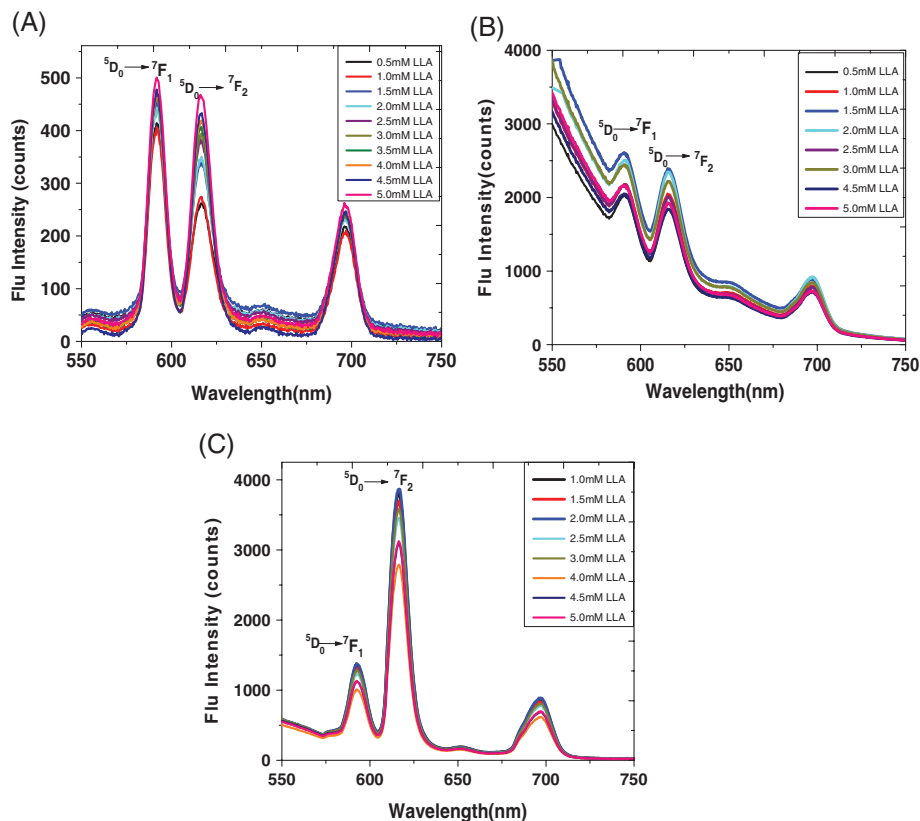
FIGURE 7   Visible fluorescence emission spectra of various concentrations of (A) L-lactic acid (LLA) in 1 mM Eu(NO₃)₃.6H₂O, (B) L-lactic acid in 1 mM Eu(NO₃)₃.6H₂O and serum and (C) L-lactic acid in 1 mM Eu(NO₃)₃.6H₂O and plasma

Eu(NO$_3$)$_3$.6H$_2$O and HBT with a linear function (integrated $0.45 \leq$ PLIR ≤ 0.95).

The calibration curve shown in Figure 8A suggests that PLIR varies exponentially and increases with lactic acid concentration, which is in agreement with what had been reported previously by Pal et al. [22] and Yu et al. [24] for lactate analysis of prostate or seminal fluids and citrate in diluted prostate fluid. The PLIR values obtained in this study at various concentrations are approximately related to Pal et al. measurements, even though Pal et al. [22] and Butler and Parker's [23] study utilized the intensity ratio of the emission peak occurred at 616/686 or 613/619 or 613/622 or 692/619 to develop the calibration curves for lactate and citrate. An important difference from the previous study is the use of luminescence emission band centered at 616 nm, which is more sensitive to change in coordination environment, and the emission peak centered at 592 nm, which is unaffected by the changes in chemical surroundings. Butler and Parker [23] demonstrated that Eu and Tb bind to bicarbonate or citrate anions in water were the only samples which show a large change in the emission spectral in lower concentration range (≤ 10 mM) by adding HCO$_3^-$. However, anions such as lactate were only detectable in concentrations ranging from 10 to 100 mM in the presence of up to 100 mM citrate using the [EuL]$^{9-}$ complex [23]. This indicates that bonding of [EuL]$^{9-}$ with lactate at lower concentration was unstable, therefore, their inability to notice any variation in emission spectral as compared to this studies. In this study, Eu^{3+}-conjugated lactate in aqueous solution revealed a significant variation in

emission spectral intensity at different concentrations ranging from 1 to 5 mM as shown in Figure 8A, signifying very low detection limit, as well as easy to use approach without using any rare earth complexes.

On the contrary, Figure 8B,C illustrates the calibration recorded for different concentrations of lactic acid in serum and plasma, which are indeed quite different from Figure 8A in terms of PLIR values. These noticeable differences in PLIR observed between the biological fluids calibration curves is attributed to low affinities of the serum, plasma and HBT binding to same site in the Eu^{3+} ion as compared to aqueous solution. For instance, very high PLIR value of the plasma, which ranges from 2.50 to 2.75, indicates a strong deformation of the symmetry around the Eu^{3+} ion, and the water molecules surrounding the Eu^{3+} ion have been replaced. Henceforth, this may signify the absence of inversion center. In case of serum, the PLIR less than 1, signifying idealized symmetry around the Eu^{3+} ion than plasma, specifies the presence of isotropic environment. This indicates that Eu^{3+} ion environment is surrounded by water molecules, and is coordinated to the OH stretching frequencies which lead to multiphonon relaxation [40]. Thus, the presence of OH vibration in the neighbor shell of the Eu^{3+} ion plays a significant role in the luminescence quenching. Also, the PLIR does not change so much with adding the lactate in both biological fluids (serum and plasma), indicating that the lactate seems not to change the Eu^{3+} ion complexation state. The decrease in PLIR value in serum and plasma can also be attributed to different microenvironments and interaction between these biological fluids
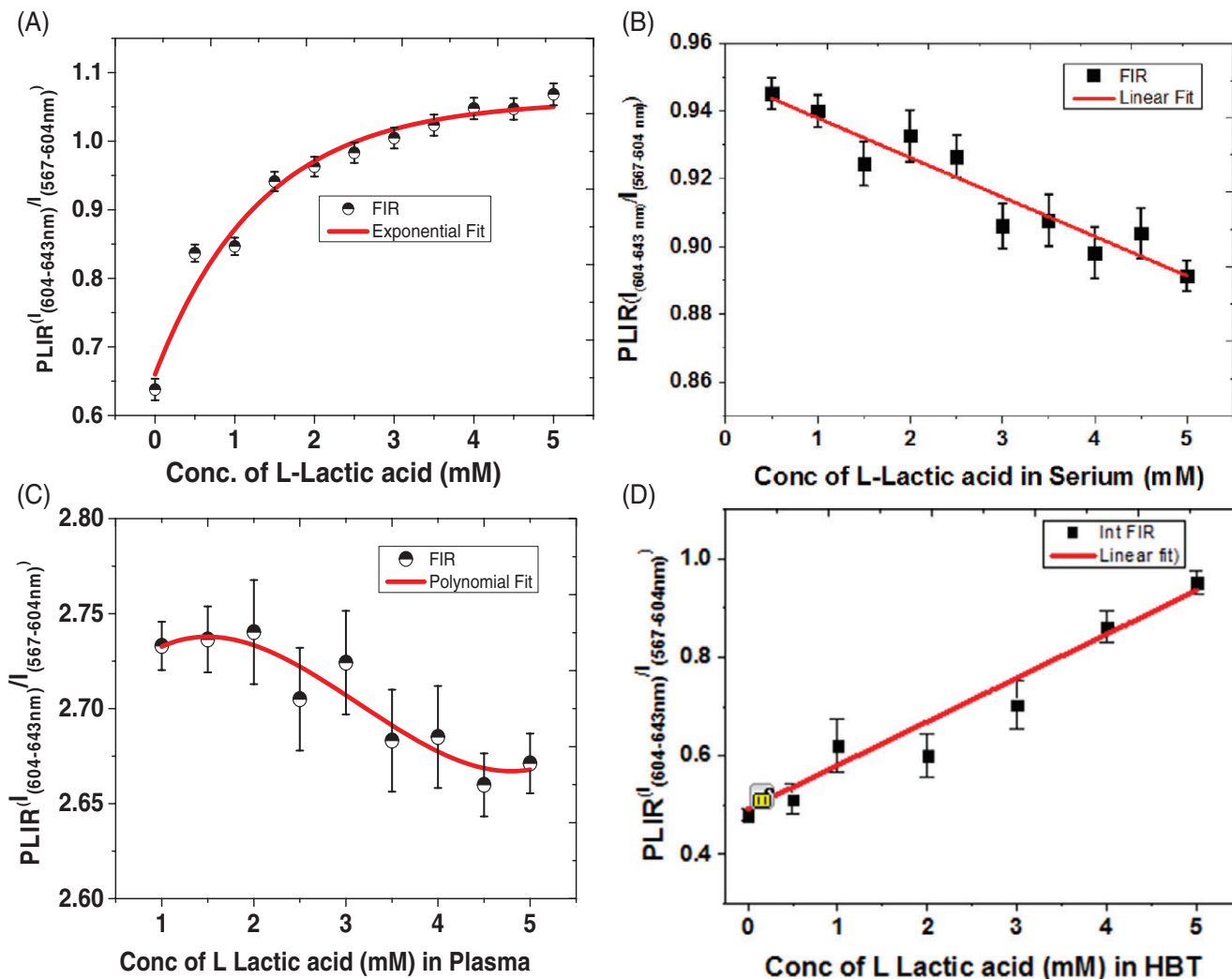
FIGURE 8 Calibration curves of lactic acid (A) integrated PLIR vs concentration of L-lactic acid (mM) in $Eu(NO_3)_3.6H_2O$, (B) integrated PLIR vs concentration of L-lactic acid (mM) in 1 mM $Eu(NO_3)_3.6H_2O$ and serum, (C) integrated PLIR vs concentration of L-lactic acid (mM) in 1 mM $Eu(NO_3)_3.6H_2O$ and plasma and (D) integrated PLIR vs concentration of L-lactic acid (mM) in 200 µM $Eu(NO_3)_3.6H_2O$ and homogenized brain tissue (HBT)

and the Eu^{3+} ion environment. For instance, Figure 8C shows the effect of increasing lactic acid concentrations in the plasma fluid on the PLIR values of the Eu^{3+} ion transitions centered at 596 and 616 nm. This could be due to difference in concentration and interaction between other metal ions (eg, potassium and sodium) in the biological fluid. Thus, causing change in the local environment of the Eu^{3+} ion and then decreasing the PLIR values. Furthermore, the overall luminescence intensity is much higher in plasma than with serum and lactate. In case of brain tissue, the PLIR starts at ~0.5 (related to the Eu^{3+} aqua ion) and increases with rising lactate concentration (as in Figure 8A), indicating that the brain tissue does not show binding behavior to Eu^{3+} ion. The integrated PLIR plotted in Figure 8 can be used to calibrate the image at concentration levels in the millimolar range in different media. For instance, the image will be yellowish in the case where the integrated intensity ratio is less than 1.0 (PLIR < 1.0),

whereas integrated PLIR greater than 1.0 (PLIR > 1.0) will exhibit reddish fluorescence image.

The confocal laser fluorescence images were recorded in the 570 to 650 nm wavelength range where the 2 characteristic peaks of Eu^{3+} were observed in the fluorescence spectroscopy. Figure 9A-D shows the confocal fluorescence image of lactic acid, HBT, Eu^{3+}-conjugated lactic acid and Eu^{3+} doped in HBT under 405 nm (which is within the 394 nm excitation band shown in Figure 5) laser excitation. The confocal fluorescence images of only lactic acid and only HBT do not show any fluorescence in the 570 to 650 nm wavelength range as shown in Figure 9A,B, respectively. The image of lactic acid conjugated with Eu^{3+} is predominantly reddish (marked regions 1 and 2) in color when lactic acid is greater than 1 mM concentration as in Figure 8A. Figure 9C demonstrates this spectroscopic image in those regions where the lactic acid forms complexes with Eu^{3+} ions. When lactic acid concentration is low, the Eu^{3+}
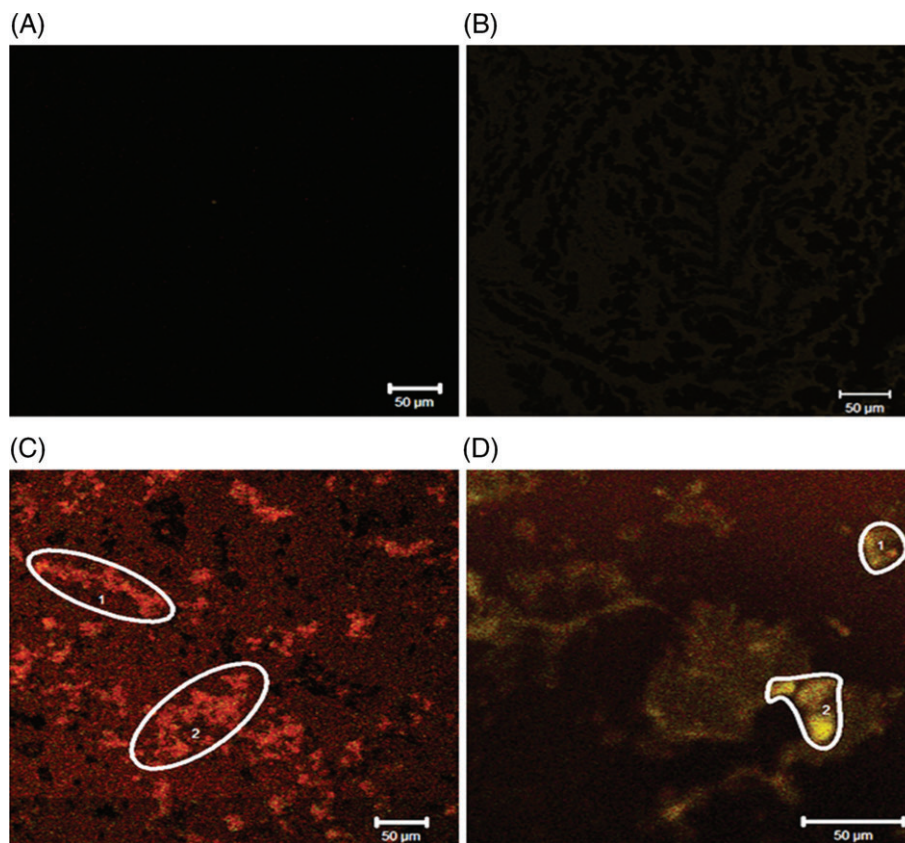
FIGURE 9 Confocal laser scanning microscope images of (A) lactic acid (control), (B) homogenized brain tissue without Eu^{3+}), (C) Eu^{3+}-conjugated lactic acid and (D) Eu^{3+} conjugated homogenized brain tissue

emission will be more yellowish and this is demonstrated in regions 1 and 2 of HBT in Figure 9D. This also agrees with the calibration data in Figure 8D where the linear increase in PLIR is observed with increase in concentrations of lactic acid but is predominantly yellowish up to 5 mM when 200 μM of $Eu(NO_3)_3$ is used as the assay.

4 | CONCLUSION

The present study demonstrates the application of visible PL of Eu^{3+} resulting from ^5D_m to ^7F_n transitions for rapid detection of lactic acid in biological samples (serum, plasma and brain tissue). The cell viability studies show that europium nitrate up to 1000 μM concentrations are safe and to some extent cytoprotective. Calibration curves of lactic acid in 1 mM $Eu(NO_3)_3.6H_2O$ and various biological fluids were constructed using rapid fluorescence measurements. The uniqueness of the integrated Eu^{3+} PLIR reported for L-lactic acid in the current study could be used as a bioimaging tool and then extended to other different metabolites released at disease states. This method could be extended for early diagnosis of chronic diseases by detecting metabolites noninvasively through superficial blood vessels and carotid artery by the use of skin-safe laser wavelengths. One of the main advantages of using lanthanides is that they have a long-lived emission which can be used to help distinguish this emission from background signals (eg, autofluorescence or scattering of the excitation laser from biological fluids or tissue). Moreover, fluorescence emission

spectra from different lanthanides may be differentiated using appropriate filters which may lead to the development of simultaneous detection and imaging of 2 or more metabolites in a single sample. Therefore, the proposed methodology of using PLIR ratio can be applied for concentration profiling and biosensing of lactic acid in tissues as well. However, further studies are needed to understand the cofounding effects of other components in the HBT on Eu^{3+} ions.

AUTHOR BIOGRAPHIES

Please see Supporting Information online.

ORCID

Eric Kumi-Barimah http://orcid.org/0000-0003-4841-9866

REFERENCES

[1] World Health Organization. Fact sheet: the top ten causes of death, http://www.who.int/mediacentre/factsheets/fs310_2008.pdf, (Fact sheet No 310) (accessed: May 2011).

[2] D. L. Longo, A. S. Fauci, D. L. Kasper, S. L. Hauser, J. L. Jameson, J. Loscalzo Eds., The Pathogenesis, Prevention, and Treatment of Atherosclerosis (Part 10, Section 5, Chapter 241). in Harrison's Principle of Internal Medicine, The McGraw-Hill Companies, New York 2012.

[3] B. Phypers, J. Pierce, *Contin. Educ. Anesth. Crit. Care Pain* **2006**, *6*, 128.

[4] J. Blumberg, *J. Nutr.* **2004**, *134*(11), 3188S.

[5] C. Waterhouse, *Cancer* **1974**, *33*(1), 66.

[6] C. K. Garcia, J. L. Goldstein, R. K. Pathak, R. G. Anderson, M. S. Brown, *Cell* **1994**, *76*, 865.

[7] F. Addabbo, B. Ratliff, H.-C. Park, M.-C. Kuo, Z. Ungvari, A. Ciszar, B. Krasnikof, K. Sodhi, F. Zhang, A. Nasjletti, M. S. Goligorsky, *Am. J. Pathol.* **2009**, *174*, 34.

[8] M. Fillenz, *Neurochem. Int.* **2005**, *47*, 413.

[9] C. J. Pepine, W. W. Nichols, *Clin. Cardiol.* **2007**, *30*, 1.

[10] S. Edwards, *Prof. Nurse* **2003**, *18*, 11636.

[11] S. Dhup, R. Kumar Dadhich, P. Ettore, P. Sonveaux, *Curr. Pharm. Des.* **2012**, *18*, 1319.

[12] A. S. Jaffe, L. Babuin, F. S. Apple, *J. Am. Coll. Cardiol.* **2006**, *48*, 1.

[13] C. Blessing, U. Feine, L. Geiger, M. Carl, G. Rassner, G. Fierlbeck, *Arch. Dermatol.* **1995**, *131*, 1394.

[14] E. Pauwels, E. Sturm, E. Bombardieri, F. Cleton, M. Stokkel, *J. Cancer Res. Clin. Oncol.* **2000**, *126*, 549.

[15] J. Zhong, S. Yang, L. Wen, D. Xing, *J. Control Release* **2016**, *226*, 77.

[16] J. Zhong, L. Wen, S. Yang, L. Xiang, Q. Chen, D. Xing, *Nanomedicine* **2015**, *11*, 1499.

[17] M. Xu, L. V. Wang, *Rev. Sci. Instrum.* **2006**, *77*, 041101.

[18] J.-C. G. Bünzli, *Acc. Chem. Res.* **2006**, *39*, 53.

[19] S. Faulkner, S. J. A. Pope, B. Burton-pye, *Appl. Spectrosc. Rev.* **2005**, *40*, 1.

[20] L. C. Courrol, F. R. De Oliveira Silva, L. V. G. Tarelho, L. Gomes, N. D. Vieira Junior, *Proc. SPIE* **2005**, *5704*, 228.

[21] G. Tian, L. R. Martin, L. Rao, *Inorg. Chem.* **2010**, *49*, 10598.

[22] R. Pal, D. Parker, L. C. Costello, *Org. Biomol. Chem.* **2009**, *7*, 1525.

[23] S. J. Butler, D. Parker, *Chem. Soc. Rev.* **2013**, *2013*(42), 1652.

[24] J. Yu, D. Parker, *Chem. Commun.* **2005**, 3141.

[25] J.-C. Bünzli, *Nat. Chem.* **2010**, *2*, 696.

[26] R. Naccache, E. M. Rodríguez, N. Bogdan, F. Sanz-Rodríguez, M. Cruz, Á. Fuente, F. Vetrone, D. Jaque, J. García Solé, J. A. Capobianco, *Cancer* **2012**, *4*, 1067.

[27] D. K. Chatterjeea, A. J. Rufaihaha, Y. Zhang, *Biomaterials* **2008**, *29*, 937.

[28] D. A. I. Junli, D. U. Peng, X. U. Jiadan, X. U. Chaoxiang, L. U. O. Laihui, *J. Rare Earths* **2015**, *33*, 391.

[29] N. J. Webster, K. N. Green, C. Peers, P. F. Vaughan, *J. Neurochem.* **2002**, *83*, 1262.

[30] F. Feyerabend, J. Fischer, J. Holtz, F. Witte, R. Willumeit, H. Drücker, C. Vogt, N. Hort, *Acta Biomater.* **2010**, *6*, 1834.

[31] C. Lizon, P. Fritsch, *Int. J. Radiat. Biol.* **1999**, *75*, 1459.

[32] M. Bishai, S. De, B. Adhikari, R. Banerjee, *J. Biotechnol.* **2015**, *5*, 455.

[33] J. R. Albani, *Principles and Applications of Fluorescence Spectroscopy*, Blackwell Science, Oxford **2007**, p. 94.

[34] S. Handy, *Applications of Ionic Liquids in Science and Technology*, In Tech, Rijeka, Croatia **2011**, p. 401.

[35] L. D. Plant, J. P. Boyle, I. F. Smith, C. Peers, H. A. Pearson, *J. Neurosci.* **2003**, *23*, 5531.

[36] K. Binnemans, *Coord. Chem. Rev.* **2015**, *295*, 1.

[37] F. S. Richardson, *Chem. Rev.* **1982**, *82*, 541.

[38] W. Carnall, P. Fields, K. Rajnak, *J. Chem. Phys.* **1968**, *49*, 4450.

[39] A. F. Kibby, D. Foster, F. S. Richardson, *Chem. Phys. Lett.* **1983**, *95*, 507.

[40] A. P. Ramos, R. R. Goncalves, O. A. Serra, M. E. D. Zaniquelli, K. Wong, *J. Lumin.* **2007**, *127*, 461.